Screening of polymer type and chemical weathering in macro and mesoplastics found in lake and river beaches using a combined chemometric approach

Nicolas Nayrac [1], Jean-Philippe Bellenger [1], Pedro A. Segura [1,*]

* Tel: 1-(819) 821-7922. Fax: 1-(819) 821-8019. E-mail: pa.segura@usherbrooke.ca
[1] Department of Chemistry, Université de Sherbrooke, Sherbrooke, QC J1K 2R1

The final version of this paper was published in Analytical Methods:
Nayrac N., Bellenger J.-P., Segura P. A. (2022): Screening of polymer type and chemical weathering in macro and mesoplastics found in lake and river beaches using a combined chemometric approach. *Anal. Methods*. https://doi.org/10.1039/D2AY01201D

Abstract

In the environment, synthetic polymers, commonly known as "plastics" are well known to undergo various chemical weathering processes which modify their surface chemistry by introducing new functional groups. Such changes are important to monitor, as they can severely influence the toxicity caused by plastic debris. Therefore, in this study, two chemometric models are proposed to accelerate the chemical classification of macro and mesoplastics found in the environment. For this purpose, principal component analysis (PCA) and hierarchical cluster analysis (HCA) were applied on preprocessed infrared spectra of 83 plastic fragments found in public lake and river beaches. HCA associated all beach samples to a known plastic whereas PCA enabled the association of only 39.8% (33 out of 83) of the beach samples to a known plastic. However, both techniques agreed on 93.9% of the samples identified. According to PCA and HCA results, polypropylene and polyethylene were the most frequently identified polymers in the samples. PCA turned out to be a very promising tool for fast screening of weathered plastics, since distance of samples from the polypropylene cluster in the PCA plot was correlated to weathering. This was later confirmed by employing other characterization techniques such as micro-Raman, X-ray photoelectron spectroscopy and scanning electron microscopy. Finally, future experiments should focus on the applicability of the proposed combined chemometric approach for very small microplastics (<100 μm), as they have more important effects than larger plastics on aquatic ecosystems.

Keywords: Multivariate analysis, plastics, Fourier-transform infrared spectroscopy, environmental fate, degradation, beach litter

1. Introduction

Since the beginning of synthetic polymer production, commonly referred as plastic, in the early 1950s, large amounts of debris of these compounds have been reported in multiple environmental compartments : surface waters [1, 2], sediments [3]; soils [4, 5], air [6], and even Arctic ice[7]. During their life span, plastic litter may undergo various environmental stresses such as mechanical abrasion, UV-irradiation, thermo-oxidation and biodegradation. All these weathering processes induce the fragmentation of macroplastic items (size >25 mm) into mesoplastics (5 mm to 25 mm), then microplastics (1 µm to <5 mm) and finally nanoplastics (<1 µm).

In the environment, these plastic fragments can act as sorbents and carriers of organic contaminants. Mato, *et al.* [8] reported an adsorption coefficient of up to 10^6, when comparing the concentrations of polychlorinated biphenyls detected on polypropylene (PP) pellets to that measured in seawater samples. While it is not clear yet whether the combined effects of plastics and associated contaminants are antagonistic or synergistic towards biota [9-12], there is no doubt that polymer type is among the most environmentally relevant properties of plastics along with size, shape and concentration, since it influences the interaction of plastic fragments with other compounds [13, 14]. For example, rubbery polymers, such as polyethylene (PE) and polypropylene (PP) have more flexible chains than glassy polymers such as polyvinyl chloride (PVC), polystyrene (PS), and polyethylene terephthalate (PET). Therefore, in the former the greater chain mobility results in better diffusion of organic compounds within the polymer matrix than in the latter [15]. Similarly, plastics with high degrees of crystallinity tend to have low sorption capacities since only their amorphous fractions can interact effectively with organic compounds [14].

Moreover, weathering of plastics can change their sorption capacity towards chemical contaminants [16]. Liu, *et al.* [17] observed that the sorption capacity of PS and PVC particles (≈ 75 µm) for polar ciprofloxacin ($\log K_{ow} = 0.4$) was increased by 123.3% and 20.4%, respectively, after a photooxidation period of 96 h. Wu, *et al.* [18] reported a threefold increase in the sorption capacity of isotactic PP towards triclosan ($\log K_{ow}=4.76$) following a 40-day period of heat-activated treatment with potassium persulfate. In both cases, these changes were explained by the polymer surface oxidation resulting from weathering. Therefore, adsorption resulting from hydrogen-bonding or electrostatic interactions enhanced the surface affinity of PP for hydrophilic contaminants.

For the reasons mentioned above, characterization of plastic fragments is essential to better understand their ecotoxicological risks. Up to now, several instrumental techniques have been used to identify the polymer type of plastic fragments found in the environment. The two most common types of molecular spectroscopy cited in the literature are Fourier-transform infrared (FTIR) and Raman spectroscopies [19-22]. Relative to FTIR spectroscopy, Raman spectroscopy is more sensitive to non-polar functional groups (e.g., C=C bonds), offers a better spatial resolution (down to 500 nm compared to 10-20 µm in the case of FTIR) and displays narrower spectral bands [23]. However, such advantages can be severely hampered by some hurdles, as this method has an inherently low signal-to-noise ratio which is prone to fluorescence interferences. As for FTIR, it also has a few limitations according to the acquisition mode used, e.g., breakup of non-mechanically stable samples, high background absorption [24] and reflection errors due to uneven surfaces. A recent review showed that, out of 40 studies conducted on analysis of microplastics in water and sediments, 50% of them used FTIR-based techniques and 10% Raman spectroscopy [21]. Also, Cowger, *et al.* [22] arrived at a similar conclusion. In studies published between 1995 and 2019 where the chemical nature of plastic samples was assessed, FTIR was the most common spectroscopic technique (57%), followed by Raman spectroscopy (21%).

Nowadays, commercial instruments use searching algorithms to compare the preprocessed FTIR spectra to a commercial or customized reference library by calculating the *hit quality index* (HQI) and by setting a threshold value, generally ≥ 70%, above which a polymer type is assigned to a sample [25]. Even though this approach is adequate for relatively pristine plastics, it may not be suitable for those that are highly weathered and have a surface in an advanced oxidation state. More recently, open-access libraries have become available for Raman spectroscopy [26] and ATR-FTIR [27, 28]. De Frond, *et al.* [27] demonstrated that including a library composed of environmentally aged plastics in addition to a commercial library allowed for an improved spectral matching success rate and accuracy. Since such libraries are still in their infancy (only a few hundred on entries), alternative methods to identify polymer type and weathering are needed.

An alternative approach to identify polymers in the environment is multivariate classification models such as principal component analysis (PCA), hierarchical cluster analysis (HCA), partial least squares – discriminant analysis or soft independent modelling by class analogies. Their role in accelerating small microplastics (< 100 µm) identification when coupled to infrared imaging has gained more attention in the past years, [e.g., da Silva, *et al.* [29]]. Likewise, Primpke, *et al.* [28] used HCA of FTIR reference spectra to detect microparticles as small as 11 µm, highlighting the great advantages of coupling multivariate techniques to µ-FTIR imaging. More recently, a proof-of-concept was established for illustrating the power of using PCA in combination to ATR-FTIR to assess the UV-B photodegradation mechanisms of a set of common plastics [30]. By reducing the dimensionality of the ATR-FTIR dataset, PCA was able to display the effects of photochemical aging of four plastics. Thus, combining chemometric tools to FTIR spectroscopy appears to be a very promising alternative to conventional library searching.

The objective of the present work is to elucidate the chemical nature and signs of weathering of polymer debris found in lake and river beaches by applying FTIR spectroscopy in combination with two chemometric techniques (PCA and HCA). The results obtained were then validated by three other characterization techniques (micro-Raman, X-ray photoelectron spectroscopy and scanning electron microscopy) to confirm the polymer type and the surface changes induced by weathering.

2. *Experimental*

Details on the reagents, materials and methods used are provided according to microplastics analysis reporting standards proposed by Andrade, *et al.* [31] and Cowger, *et al.* [32].

2.1. Reagents and materials

Standards of low-density polyethylene [ρ=0.92 g mL^{-1} at 25 °C, average molecular weight (MW)=4,000 Da, Product number : 427772], medium density polyethylene (ρ=0.94 g mL^{-1} at 25 °C, 332119), isotactic polypropylene (ρ=0.9 g mL^{-1} at 25 °C, MW=12,000 Da, 428116), amorphous polypropylene (ρ=0.9 g mL^{-1} at 25 °C, 428175), polystyrene (ρ=1.06 and 1.047 g mL^{-}

^{1} at 25 °C, MW=35,000 Da and MW=280,000 Da, 331651 and 182427 respectively), polyvinylchloride (ρ=1.4 g mL^{-1} at 25 °C for both, MW=48,000 Da and 85,000 Da, 81388 and 182621 respectively) and polyethylene terephthalate (ρ=1.68 g mL^{-1} at 25°C, 429252) were all purchased from Sigma-Aldrich. Please note that physical properties for standards were reported as stated by the supplier.

Polymer samples derived from diverse consumer products (e.g., food containers, bottles, etc.) were also gathered for analysis. Only samples indicating the polymer nature with recycling codes were used. In total 22 consumer product samples were collected: 8 polyethylene samples (PE) (yogurt, nutrients/vitamin bottle), 10 polypropylene samples (PP) (yogurt, shovel, flowerpot), 10 polyethylene terephthalate samples (PET) (energy drink, food container), 10 polystyrene samples (PS) (yogurt, coffee cup, foam) and 8 polyvinylchloride samples (PVC) (gloves, tubes). Depending on the ease of cutting, several sizes were obtained, all in the mesoplastic range (i.e., 5 mm – 25 mm). This was done with the aid of a metal cutter. Samples were also further checked by ATR-FTIR to ensure that they presented no evident signs of chemical weathering. For that purpose, three distinct spots were analyzed on the outer surface of each material and then averaged.

Control samples, including acrylonitrile butadiene styrene (ABS, *n*=1, Lego brick), polycarbonate (PC, *n*=1, roof plate), polytetrafluoroethylene (PTFE, *n*=1, round tube), polyamide (PA, *n*=1, unknown origin) and polyurethane (PU, *n*=1, insulation foam), were also used to evaluate the selectivity of the method.

2.2. Sample collection and preparation

Samples of polymer fragments were picked up by hand in four different beach locations in the Estrie region in Quebec, Canada between June and August 2019, during sunny days. Four different locations were sampled at least three times: Lyster lake beach (latitude 45.0337674 N; longitude -71.9189507, sampling dates: 07/23/2019, 08/062019 and 08/13/2019), Magog City public beach (45.294228; -72.0451747, 07/23/2019, 08/06/2019 and 08/13/2019), Municipal beach in Sherbrooke (45.3355837; -72.0239399, 07/23/2019, 08/06/2019 and 08/13/2019) and Lucien Blanchard Park beach in Sherbrooke (45.3929262; -71.9381494, 06/21/2019, 07/23/2019 and 08/13/2019).

After collection, samples were stored in the dark at room temperature in Petri dishes until further use. All samples (i.e., standards, consumer products, control, and beach samples) were rinsed prior to analysis, in a vacuum filtration system, as follows: three times with distilled de-ionized water, twice with water purified by Milli-Q system, once with ethanol (95% volume, P016EA95, Greenfield), once with hexane (ACS reagent ≥98.5%, 178918, Sigma-Aldrich) and finally one time with methanol (≥99.9%, A456-4, Fisher).

In a recent study by Kirchkeszner*, et al.* [33], it was demonstrated that ethanol 95% *v/v* caused swelling of PP and increased the concentration of additives at the polymer surface. Thus, swelling processes could potentially alter the chemical characterization of polymers. However, such phenomenon is limited (<1% of swelling) when contact times are low (< 25 h) at it is the case for the rinsing and cleaning procedure used here, which lasted only a few minutes per sample. Since the presence of artifacts (e.g., biofilms, organic matter) on polymers' surfaces can also alter their chemical characterization, cleaning procedures using organic solvents are necessary.

2.3. Attenuated total reflectance-Fourier-transform infrared (ATR-FTIR) spectroscopy

FTIR spectra were acquired on a Cary 630 Agilent spectrometer using the single-bounce ATR mode. Samples were placed on a diamond crystal plate and scanned from 600 cm^{-1} to 4000 cm^{-1} at room temperature. Data was collected as transmittance percentage (T%, y axis). Spectral resolution was set to 4 cm^{-1} and 32 accumulated scans per sample. An HappGenzel apodization function (Agilent microLab software) was applied for each spectra recorded. Background settings were the same as for sample analysis, with the difference that no load was placed against the crystal. Moreover, special care was taken to record the background before measuring each sample, to decrease as much as possible external error sources (e.g., breathing, atmospheric variability) which could have a direct influence on the spectral shape and the chemometric analysis. Additionally, all spectra were corrected for light-reflectance penetration and baseline displacement. For some rough plastics, it was impossible to directly obtain a reproducible signal due to geometrical irregularities. Therefore, these samples were cut with a metal cutter in such a way that made the surface flatter. This procedure allowed for the analysis of all beach samples.

Samples collected in Lucien Blanchard Park beach (73.5 % of the collected samples) were analyzed in triplicate to confirm the absence of intra-sample variability, poor contact between the sample and ATR element and/or atmospheric variability. After checking the data collected, it was concluded that spectra were reproducible, and the rest of the samples were analyzed only once.

2.4. Data analysis

Once spectra were obtained, data preprocessing was necessary to remove noise and enhance small differences between the spectra of the samples given their structural similarities [34]. For example, the presence of methylene groups in all polymers or the occurrence of phenyl groups in both PS and PET. Therefore, a series of transformations were applied on FTIR spectra, in accordance with a previously validated method [35].

First, the FTIR spectra collected in triplicate were averaged and standardized (i.e., by subtracting the mean from an individual transmittance value and then dividing the difference by the standard deviation). Then, the first derivative of each spectrum was calculated and a Savitzky-Golay smoothing (second-order polynomial, points of window: 5) was applied. All preprocessing steps were done in OriginPro software (version 2021b) from OriginLab. The spectra thus preprocessed were then analyzed using PCA and HCA also using OriginPro.

For PCA, the Principal Component Analysis for Spectroscopy (v.1.30) application in OriginPro was used. Wavenumbers (4000-600 cm^{-1}, in total 1825 different values) were set as variables and preprocessed signal for each sample as observations. In the Settings tab, the first 10 principal components (PCs) were extracted using the covariance matrix. Likewise, the "Standardize Scores" option was selected to standardize scores of each component. In the "Quantities to Compute" tab, Loadings and Scores were selected, and their values reported in the report data sheet. In the "Plots" tab, Scree plot, loading Plot, score plots and biplots were created to investigate the relationships between variables and observations. Confidence ellipses were also shown to spatially visualize which samples should be considered as classified and others whose identity remained unknown. Finally, all plots (except Scree plots) were given in a two-component configuration as the inclusion of a third component would have rendered any interpretation of results too complicated.

In the case of HCA, wavenumbers (4000-600 cm^{-1}, 1825 different values) were set as observations and preprocessed signals for each sample as variables. In the "Settings" tab, variables were selected as the type of objects to cluster. Furthest neighbor, also known as complete linkage, was set as the cluster method. Pearson correlation was used as distance type and the sum of squares of distances was used to find clustroids, i.e., the most representative data point for each cluster. Variables were standardized with zero mean and unit standard deviation in the preprocessing step so as no more standardization was necessary prior to HCA analysis. The number of clusters was set to six considering the number of targeted polymers (PE, PP, PS, PVC, and PET) plus an "unknown" group. Increasing the number of clusters to ten, did not change significantly the dendrogram. In the "Quantities" tab, dissimilarity matrix, cluster stages and clustroid info were selected and the calculated values reported in a new data sheet. In the "Plot" tab, results were displayed in a single graph in the form of a circular dendrogram with the y axis indicating the distance between two variables. Other types of distances (i.e., Euclidean, city block [Manhattan)] and cosine distances) were tested (Microsoft Excel sheet DissimilaryMatrices.xlsx, Supplementary information) but better results were obtained with Pearson correlation. Likewise, the ability of clustering methods (i.e., nearest neighbor, furthest neighbor, group average and ward) to generate of new clusters was tested. Except for nearest neighbor, no variation was observed in the classification of variables.

2.5. Micro-Raman (μ-Raman) spectroscopy

μ-Raman spectra were acquired on a Horiba LabRam HR800 (Jobin Yvon) system equipped with a nitrogen-cooled CCD detector and working in a backscattering configuration. Samples were excited by a He-Ne laser emitting at 632.8 nm wavelength with a laser power kept at 2 mW. For every sample, the optimum integration time was set at 2 min and the cumulation number was set at 10. In this way, a good signal/noise ratio was obtained, and cosmic rays were removed. Spectra were collected in the 560 – 3300 cm^{-1} wavenumber range using 1800 lines per millimeter grating, a spectral resolution of 0.1 cm^{-1}, 50× microscope objective, a hole diameter and slit width of 300 μm and 150 μm, respectively, were used. Please note that the incident beam was focused on a spot of about 3 μm in diameter. Before starting any acquisition, samples were first visualized on a color camera by turning the white light illumination on and putting the camera beam splitter down. The instrument was calibrated using the known Si Raman band at 520.07 cm^{-1}. Once acquired, all individual spectra (wavenumber range of ~850 cm^{-1}/spectra) were manually corrected by a multiplying factor to allow for any pixel-to-pixel variation in response to be averaged out over the whole spectrum. This step was mandatory as moving the grating resulted in an offset between two consecutive spectra. Finally, Raman signals measured in counts per second (cps, y axis) were standardized in the same manner as for ATR-FTIR data. Spectra were not recorded in triplicate but three different spot positions per sample were carefully examined to avoid reproducibility issues. Other data transformations (e.g., smoothing, baseline correction) were not applied as standardization alone allowed for spectral comparisons based on expert knowledge.

2.6. X-ray photoelectron spectroscopy (XPS)

XPS spectra were acquired on an Ultra DLD spectrometer from Kratos. Sample excitation was done by an Al Kα monochromatic source (1486.6 eV) operated at 15 kV and 15 mA, with 225 W of applied power. The pressure in the analyzing chamber was maintained below 5.10^{-8} Torr during analysis and the probe sample area was set at 300 μm×700 μm. The depth of analysis was estimated to be at ≈10 nm. The photoelectrons were emitted at a 90º angle relative to the plastic surface. The analyzer was running in a constant pass energy mode (160 eV for the survey scans and 20 eV for the high-resolution scans). The work function of the instrument was calibrated to give a binding energy (BE) of 83.96 eV for the Au $4f_{7/2}$ line of metallic gold. The dispersion of the spectrometer was adjusted to give a BE of 93.62 eV for the Cu $2p_{3/2}$ line of metallic Cu. The sample was mounted on a non-conductive tape and a charge neutraliser was used on all samples to compensate for the charging effect. Charge corrections were made according to the C_{1s} core level of aliphatic polymers at 285.0 eV. Data analysis was conducted using the Casa XPS software (version 2.3.25) by CasaSoftware. The relative sensitivity factors used were those provided by the manufacturer (i.e., Kratos) and the line-shape functions were either of Gaussian-Lorentzian product form or of asymmetric type, depending on the chemical function of interest. Three types of spectra were collected: a survey spectrum and two high-resolution spectra corresponding to the C_{1s} and O_{1s} regions.

2.7. Scanning electron microscopy (SEM)

Surface images were taken using a Hitachi S-4700 field emission scanning electron microscope, with an electron accelerating voltage of 5.0 kV and a 30° sample tilt. Images were acquired at low (30×) and high (200× to 415×) magnification. Prior to SEM analysis, samples were sputtered with Au/Pd for 30 s using a Hummer 6.2 instrument from Anatech.

3. Results and discussion

3.1. Characteristics of sampled plastic fragments

In total, 83 plastic fragments were collected in the Estrie region in Quebec, Canada: 61 in Lucien Blanchard Park beach, 9 in Lyster lake beach, 4 in Magog beach and 9 in the Sherbrooke municipal beach. Globally, a consistent trend was observed for the size distribution of beach plastics, with the number of items found negatively correlated with the size, ranging from 0.3 to 7.5 cm. No tendency was noted for colors. However blue, white, and red were the most represented colors, as their proportion was comprised between 49% to 78 %, depending on the sampling site.

Regarding shape, the fragments collected had different forms: planar, curved and some of them had irregularities. Irregular shapes are frequently observed during the detection of plastic fragments with a stereomicroscope. Moreover, rough fragmented textures were discovered in many collected water and sediment samples [36-38], primarily because of mechanical and/or chemical weathering of larger plastic items. In the present case, it was difficult to make assumptions regarding the origin of the plastic debris. However, for many fragments, a well-defined shape was reported, suggesting a short-scale transport from the source. It could be either due to an improper disposal by consumers (i.e., littering) directly on site or in the vicinity, discharge via stormwater tanks during high-rain events or through wastewater treatment plants (WWTPs) effluents, although this last case seems less plausible, as macro and mesoplastics entering WWTPs are supposed to be retained during primary treatment process [39].

3.2. Chemometric analysis of preprocessed FTIR spectra to screen polymer type

3.2.1. Validation of the identification of polymer type by principal component analysis

FTIR spectra of standard samples as well as peak identification are shown in Figures S1 to S5 (Supplementary information). Acquired spectra of standards and consumer products of known composition were then preprocessed, and an example is shown in Figure S6 (Supplementary information). As it can be seen, preprocessed spectra showed a negative and positive peak for each transmittance peak since they were obtained from the first derivative of the original FTIR spectra. These spectra were then analyzed by PCA to test if standards and commercial samples of the same type could be grouped together.

Figure 1A shows biplots of the 1st principal component (PC1) vs. the 2nd principal component (PC2) and Figure 1B shows PC1 vs. the 3rd principal component (PC3). As it can be seen, polymers of the same type, regardless of their origin (i.e., standard or consumer product), formed clusters and thus can be easily differentiated from each other. The variables (in this case frequencies in wavenumber units) having a larger impact on the separation of the samples are represented as loadings (vectors) in the biplots. For sake of simplicity, only the variables with the highest loadings, i.e., with absolute values larger than half of the maximum loading value in each principal component, were included. Therefore, the vectors showed in biplots match the peaks in the preprocessed FTIR spectra that have the largest impact in segregating and grouping the samples. Confidence ellipses, based on Hoteling's T2 statistic can be employed to detect outliers in PCA [40]. For that reason, the location inside or outside the 95% confidence ellipses was used as a criterion to identify which samples can be associated with polymers of known composition.

As it can be seen in Figure 1A and Figure 1B, the presence of pairs of peaks in the preprocessed spectra has a major effect on the PCA. Biplots show pairs of positively and negatively correlated loadings to each principal component. For example, in the case of PP in Figure 1A, there is a linear dispersion which is strongly correlated to the 2nd principal component and linked to the bending vibrations of the methyl groups at 1377 cm^{-1} [19] represented by the loadings between 1379-1385 cm^{-1}.

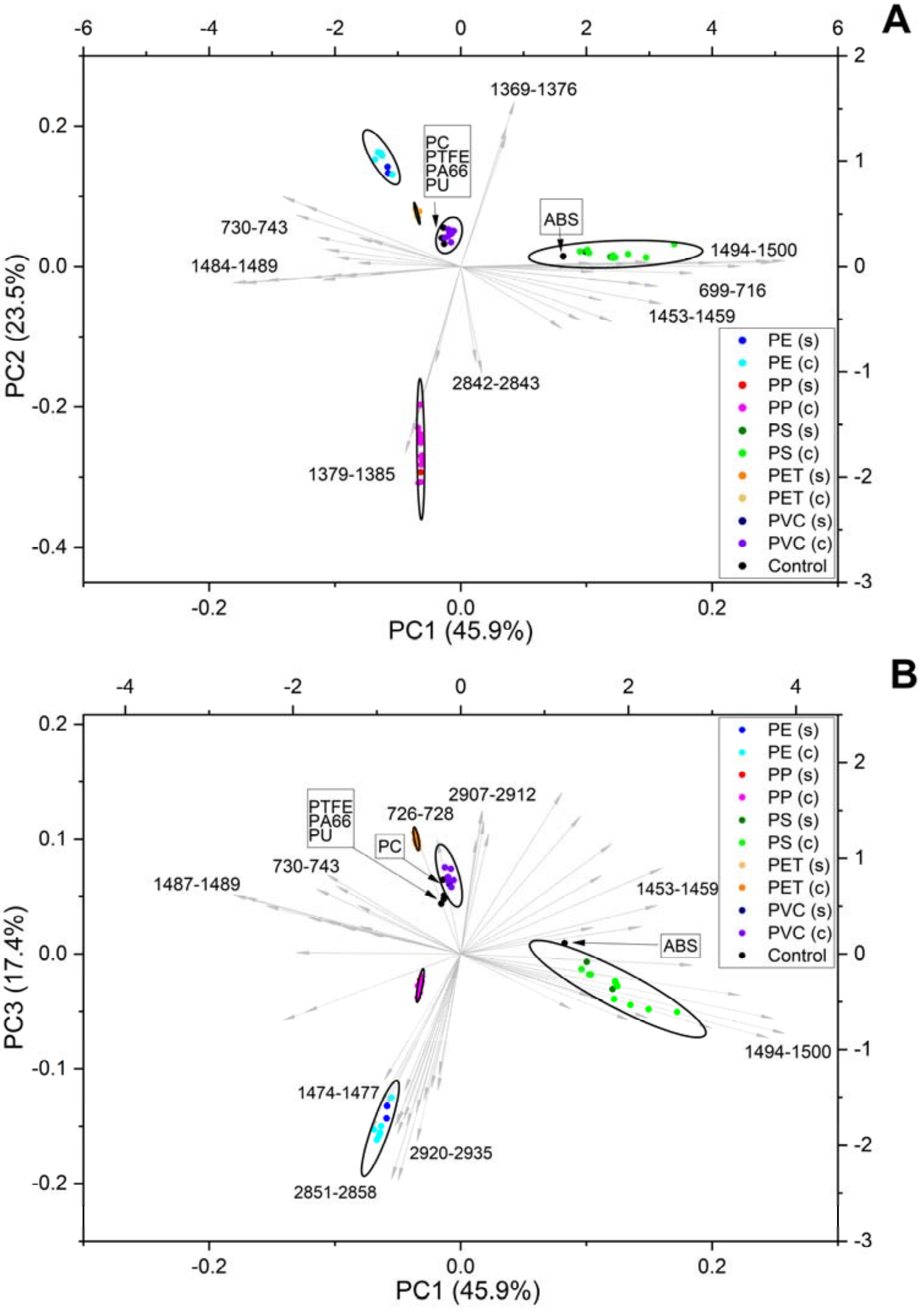

Figure 1. Biplots (A: PC1 vs PC2, B: PC1 vs. PC3) of preprocessed spectra of standards (s) and consumer product (c) polymers. PE: polyethylene, PP: polypropylene, PS: polystyrene, PVC: polyvinyl chloride and PET: Polyethylene terephthalate. Numbers besides the loadings correspond to wavenumbers with the highest coefficients for each PC. Left and bottom axes correspond to the loadings plot and right and top axes to the scores plot. Ellipses indicate 95% confidence.

Since CH_3 moieties are less abundant in PE (<2–30 CH_3/1000 C) compared to isotactic PP (333 CH_3/1000 C) [41], the segregation between these two classes of polymers was possible by PCA. Consequently, PE is rather described by other peaks in the preprocessed spectra correlated to PC2 or PC3 and ranging from 730-743 cm^{-1} (Figure 1A) and 2851-2858 cm^{-1} (Figure 1B), due to CH_2 rocking and C–H stretching, respectively. This last mode of vibration is shifted for PP as it appears in a less intense manner at lower frequencies. PS is also well separated from PE and PP because it introduces three new peaks, the two most representative being the out-of-plane aromatic C–H bending corresponding to the loadings 699-716 cm^{-1} and the skeleton vibrations of the benzene ring between 1494-1500 cm^{-1} [38].

PET and PVC clustered together near the origin in both Figure 1A and Figure 1B due to the low intensity of their raw spectra (Figure S4 and S5, Supplementary information) especially in the region comprised between 2000 and 4000 cm^{-1} compared to the other three polymers (Figures S1 to S3). Nevertheless, they were separated in both biplots as indicated by their 95% confidence ellipses. The loadings at 730-743 cm^{-1}, which are strongly correlated to PC1, enable the discrimination between PET and PVC (Figure 1A and 1B). In fact, they correspond to the aromatic bending of C-H bonds only present in PET and shifted to lower wavenumbers (699-716 cm^{-1}) in the case of PS.

Control samples (ABS, PA66, PC, PTFE, PU) were also included in the PCA biplots to test the reliability of the method. In the biplot of Figure 1A, ABS clusters with the PS samples, since this copolymer is partially composed of styrene monomeric units. However, in the biplot of Figure 1B, it is located just outside of the 95% confidence ellipse of PS. In the case of PTFE, PA66, PC and PU, despite notable differences in their raw and preprocessed spectra as shown in Figures S7 and S8 (Supplementary information), these control samples cluster with PVC in the biplot of Figure 1A. However, only PC appears inside the 95% confidence interval for PVC in the biplot of Figure 1B. This observation may be explained by the lack of meaningful signal intensities in the spectra of the control samples at the wavenumbers that explain most of the variability in PC1 and PC2 [19], which impedes their discrimination in the first biplot.

In summary, PCA of preprocessed FTIR spectra was efficient at distinguishing the most frequently detected polymers (PE, PP, PS, PET and PVC). More importantly, all polymers of a same type clustered inside the same 95% confidence ellipse, meaning that any divergence which could be later observed in case of beach plastics could potentially suggest weathering. PCA results also showed that the control sample ABS clustered inside the 95% confidence interval of PS and PA66, PC, PTFE and PU were located inside the 95% confidence interval of PVC in the PC1 vs PC2 biplot. However, this trend was not observed in the PC1 vs the PC3 biplot. Therefore, identification of polymer type by PCA of environmental samples could be less accurate for PS and PVC.

3.2.2. Screening of polymer type of beach samples by PCA

After a validation step proving the robustness and limitations of the PCA method, beach (i.e., unknown) samples were further included in the analysis. Biplots of the preprocessed FTIR spectra of plastics of known composition and beach samples are shown in Figure 2. Given the similarity between the spectra of standards and consumer products (Figure 1), they were pooled together according to polymer type (i.e., PE, PP, PS, PVC, or PET). The PCA showed that the first three PCs accounted for 87.7 % of the observed variation in the preprocessed spectra of all samples.

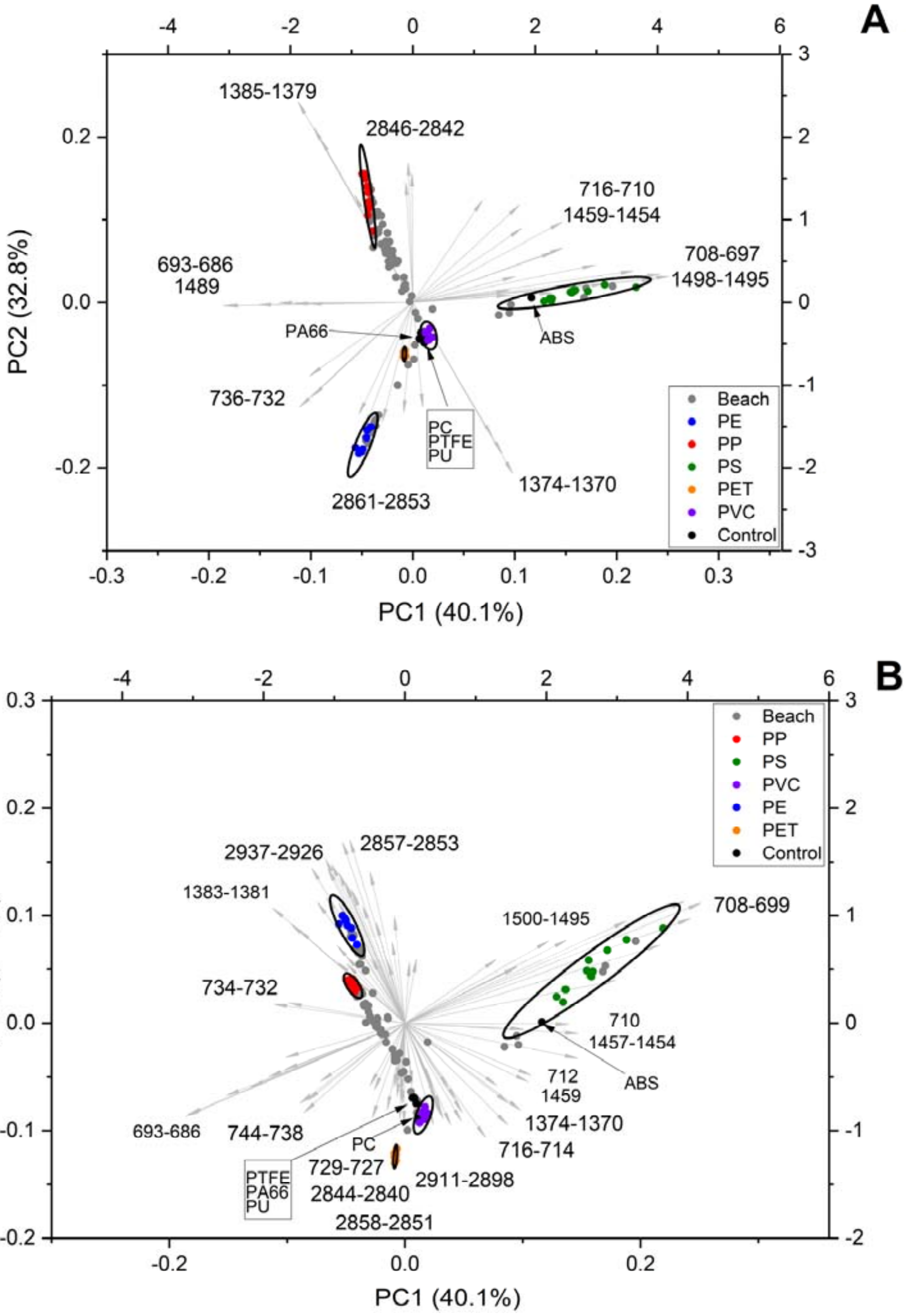

Figure 2. Biplots (A: PC1 vs PC2, B: PC1 vs. PC3) of the preprocessed FTIR spectra of polymers of known composition (standards, consumer products and controls) and samples found on beaches. PE: polyethylene, PP: polypropylene, PS: polystyrene, PVC: polyvinyl chloride and PET: polyethylene terephthalate, PU: polyurethane; ABS: acrylonitrile butadiene styrene PA66: polyamide; PC: polycarbonate; PTFE: polytetrafluoroethylene. Ellipses indicate 95% confidence. Numbers besides the vectors correspond to wavenumbers with the highest coefficients for each PC. Left and bottom axes correspond to the loadings plot and right and top axis to the scores plot.

Some beach samples clustered inside the 95% confidence ellipses of PE, PP, PS, PET, and PVC. For that reason, according to the biplot shown in Figure 2A, their relative proportions were: PE (15.7% or 13/83), PP (15.7% or 13/83), PS (4.8% or 4/83), PET (1.2% or 1/83), PVC (2.4% or 2/83). Nevertheless, it is conceivable that the beach samples inside the 95% interval ellipses of PVC or PS could be wrongly identified since control samples (PA66, PC, PTFE PU and ABS) were grouped with one of these two polymers. In just a few cases (5 out 83), there was a discrepancy between the identification given by PC1 vs PC2 and PC1 vs PC3. This observation is consistent with the very nature of PCA, where the first two PCs extract the most representative peaks of each type of polymer. The remaining beach samples (60.2%, or 50/83) could be classified as outliers.

It was hypothesized that these outliers correspond either to copolymers (i.e., polymer blends) or weathered plastic fragments, for which altered surface functional groups may have changed their infrared spectra signature. On the other hand, fragments for which a polymer type was assigned (39.8%, 33/83) should have little to no degree of chemical weathering. This behavior seems rather logical since these samples cluster with standard or commercial polymers, whose unaltered state was known. Since 60.2% beach polymers remained unidentified, another multivariate statistical method, HCA, was applied to further group the beach samples in clusters associated to polymers of known composition.

3.2.3. Hierarchical cluster analysis

Results of the HCA of samples of known composition and beach samples are shown in Figure 3. According to HCA, out of 83 beach samples, 21.7 % (18/83) could be associated to PE, 65.1 % (54/83) to PP, 7.2 % (6/83) to PS, 6.0 % (5/83) to PET, and 0% to PVC. None of the beach samples were classified as “unknown” by HCA and only two controls (PTFE and PC) were clustered apart from all the other samples. This was not due to the number of selected clusters (six) used to perform the analysis, since a higher number of clusters (e.g., ten) revealed that only four beach samples did not cluster with PE, PP, PS, PET, or PVC.

Control samples were grouped either on their own or with a polymer standard. PTFE and PC clustered in an "unknown group" while ABS was grouped with PS (the same was observed in the PCA), while PA66 and PU were grouped with PE and PET, respectively. These latter control samples were more similar to beach samples than to polymer standards or to commercial samples as they were located in different subbranches in the dendrogram. Surprisingly, no control was grouped with PVC as it was the case in the PCA. PA66 showed a $-CH_2$ stretching band at 2862 cm^{-1} like that of PE at 2870 cm^{-1}, which explains the grouping of PA66 to the PE cluster. In the case of PU, its structure shares some common structural features with PET, that is the presence of an aromatic C–H out-of-plane bending located at 817 cm^{-1} or a C–O stretching band at 1726 cm^{-1} coming from the ester group. As explained previously, ABS clustered with PS samples due to the presence of styrene monomeric units. Although PTFE and PC are different in terms of composition, they were grouped together in the dendrogram, probably because they had both strong signals in the region < 1750 cm^{-1} and weak peaks in the region > 1750 cm^{-1}.

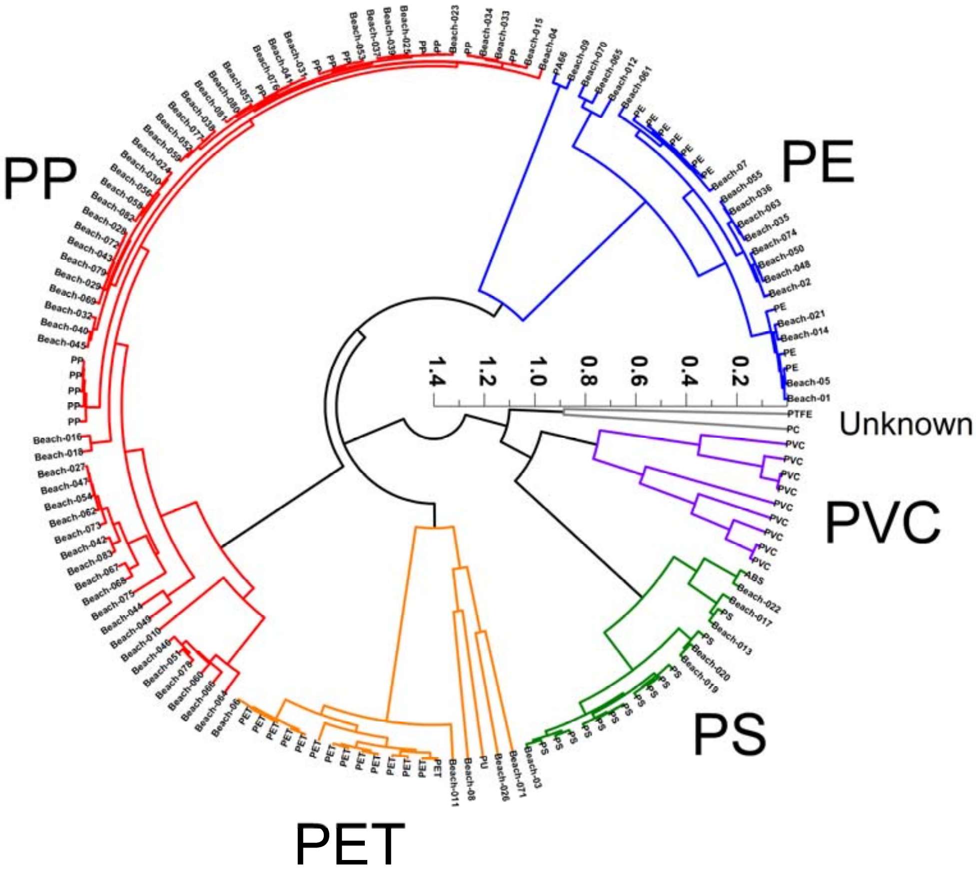

Figure 3. Circular-oriented dendrogram obtained by HCA of preprocessed FTIR spectra of standards, consumer products, controls and beach samples. The scale from 0 to 1.4 indicates distance according to the similarity among the samples. For the sake of clarity, standards, and consumer products of the same type of polymer were pooled. PE: polyethylene, PP: polypropylene, PS: polystyrene, PVC: polyvinyl chloride, PET: polyethylene terephthalate.

3.2.4. Comparison of PCA and HCA to screen polymer type

As mentioned in the previous sections, in the case of PCA, samples were assigned to a polymer type when they fell inside a 95% confidence ellipse, otherwise they were labeled as "Not Identified |(N.I.)". For HCA, the identification was made depending on the presence of standard/consumer product samples in the same branch as the beach sample. Therefore, according to the results obtained by PCA and HCA (Table 1), PE and PP are the most abundant types of polymers recovered on the samples beaches. These two polymers are also the thermoplastics with the highest annual production volume worldwide [42].

Table 1. Classification of the beach samples according to PCA and HCA

Sample	Identity PCA	Identity HCA	Sample	Identity PCA	Identity HCA	Sample	Identity PCA	Identity HCA
Beach-001	PE	PE	Beach-029	N.I.	PP	Beach-057	PP	PP
Beach-002	PE	PE	Beach-030	N.I.	PP	Beach-058	N.I.	PP
Beach-003	PS	PS	Beach-031	PP	PP	Beach-059	PP	PP
Beach-004	N.I.	PP	Beach-032	N.I.	PP	Beach-060	N.I.	PP
Beach-005	PE	PE	Beach-033	PP	PP	Beach-061	PE	PE
Beach-006	PET	PET	Beach-034	PP	PP	Beach-062	N.I.	PP
Beach-007	PE	PE	Beach-035	PE	PE	Beach-063	PE	PE
Beach-008	PVC	PET	Beach-036	PE	PE	Beach-064	N.I.	PP
Beach-009	N.I.	PE	Beach-037	N.I.	PP	Beach-065	N.I.	PE
Beach-010	N.I.	PP	Beach-038	N.I.	PP	Beach-066	N.I.	PP
Beach-011	N.I.	PET	Beach-039	PP	PP	Beach-067	N.I.	PP
Beach-012	N.I.	PE	Beach-040	N.I.	PP	Beach-068	N.I.	PP
Beach-013	PS	PS	Beach-041	PP	PP	Beach-069	N.I.	PP
Beach-014	PE	PE	Beach-042	N.I.	PP	Beach-070	N.I.	PE
Beach-015	N.I.	PP	Beach-043	N.I.	PP	Beach-071	PVC	PET
Beach-016	N.I.	PP	Beach-044	N.I.	PP	Beach-072	PP	PP
Beach-017	PS	PS	Beach-045	N.I.	PP	Beach-073	N.I.	PP
Beach-018	N.I.	PP	Beach-046	N.I.	PP	Beach-074	N.I.	PE
Beach-019	N.I.	PS	Beach-047	N.I.	PP	Beach-075	N.I.	PP
Beach-020	N.I.	PS	Beach-048	PE	PE	Beach-076	PP	PP
Beach-021	PE	PE	Beach-049	N.I.	PP	Beach-077	N.I.	PP
Beach-022	PS	PS	Beach-050	PE	PE	Beach-078	N.I.	PP
Beach-023	PP	PP	Beach-051	N.I.	PP	Beach-079	N.I.	PP
Beach-024	N.I.	PP	Beach-052	PP	PP	Beach-080	N.I.	PP
Beach-025	N.I.	PP	Beach-053	PP	PP	Beach-081	N.I.	PP
Beach-026	N.I.	PET	Beach-054	N.I.	PP	Beach-082	N.I.	PP
Beach-027	PP	PP	Beach-055	PE	PE	Beach-083	N.I.	PP
Beach-028	N.I.	PP	Beach-056	N.I.	PP			

N.I.: not identified by the chemometric technique used.

When samples were identified by PCA, HCA agreed on 93.9% of the samples (31/33). It is not clear why some samples were only identified by HCA. The high number of samples not identified by PCA (50/83) can be explained by diverse factors, such as: i) environmental degradation and/or ii) the presence of additives or copolymers. It is known that polymers can degrade by various pathways, e.g., photo-oxidation/degradation, thermo-oxidation/degradation, mechanical degradation, biodegradation and hydrolysis [43]. All these natural weathering processes are expected to alter the chemical integrity of plastics by forming hydroxyl and carbonyl groups. In one study, the six-month natural photooxidative ageing of four standard polymers (LDPE, HDPE, PP and PS) was reflected by changes in the scores position in the PCA biplot [44]. Likewise, particle surface covering by organic contaminants and/or biofilms can severely hamper the proper identification of plastic fragments. However, a thorough cleaning procedure using various solvents (section 2.2) was done before submitting the plastics to any identification method, thus limiting this contribution.

The results presented here suggest that PCA seems to be more susceptible than HCA to weathering effects on polymers. This may be explained by the way in which samples are clustered. In the case of PCA, variability on the preprocessed spectra was explained mostly by three principal components that are themselves linear combinations of the main peaks in the spectra. In the case of HCA, samples were grouped according to their distances, i.e., the similarities of their preprocessed spectra (the more similar two samples are, the lower their distance). Those distances were determined according to the Pearson correlation coefficients between the samples. Therefore, in HCA small differences between the spectra caused by a few peaks appear to have a lesser contribution to the overall result compared to PCA.

In contrast to conventional library searching, which is based on discrete similarity analysis calculations, e.g., hit quality index (HQI) or ΔHQI values between samples and reference databases, multivariate statistical models offer the opportunity to investigate the relationships between all samples in a single graph, either by reducing the dimensionality of the complex dataset in the case of PCA or by generating groups of related samples for HCA. Moreover, spectral features (e.g., additives, chemical weathering) which could have hindered the proper classification of samples are less susceptible to distort the results obtained by these two multivariate techniques.

3.3. Bond indexes of beach samples of selected beach samples to investigate their weathering state

It was decided to test the hypothesis mentioned earlier that the observed PP outliers, i.e., samples located outside the 95 % confidence ellipse of PP in the PC1 vs PC2 biplot of Figure 4A (a simplified version of Figure 2A), corresponded to weathered PP. This hypothesis was supported by the observation that these samples are found along the axis of the loadings 1385-1379 cm^{-1} which may indicate a gradual loss of methyl groups in the PP backbone following chemical weathering [45, 46]. It is known that weathering of polyolefins such as PP occurs mainly through photo-oxidation reactions, by means of oxygen and UV-light radiation below 400 nm [45]. Since alkane bonds do not absorb above 200 nm, other structural defects (e.g., vinylidene groups, ketones, hydroperoxides) introduced during the polymerization process act as chromophores. In the field of polymer testing and engineering, ratios between infrared absorption peaks, known as bond indexes, are routinely employed to evaluate polymer weathering [47, 48]. Different methods permit the assessment of those indexes, by measuring peak heights or band areas [49, 50]. However, considering only one specific peak instead of the entire set of peaks can be misleading, as numerous chemical functions are formed through photo-oxidation. To overcome this issue, the specified area under band (SAUB) method was recently proposed [51]. Therefore, to investigate possible weathering of the samples in Figure 4A, the carbon-oxygen, carbonyl and hydroxyl indexes were calculated by the SAUB method for each sample, following averaging of the three replicate spectra.

As it can be seen in Figure 4B, a positive linear relationship between the three indexes and the score distance to the PP standard is demonstrated by the Pearson correlation coefficients ($r_{\text{carbon-oxygen}}$=0. 8309, r_{carbonyl}=0.5713, $\mathrm{r}_{\text{hydroxyl}}$=0.7929). Samples further away from the PP standard show increasingly abundant signs of the presence of chemical functions observed in weathered polymers. Therefore, changes in the spectra at 1379-1385 cm^{-1} acted as a marker of weathering in the beach samples. Thus, the hypothesis proposed earlier that the beach samples outside the 95 % confidence ellipse of Figure 4A are weathered PP appears to be validated.

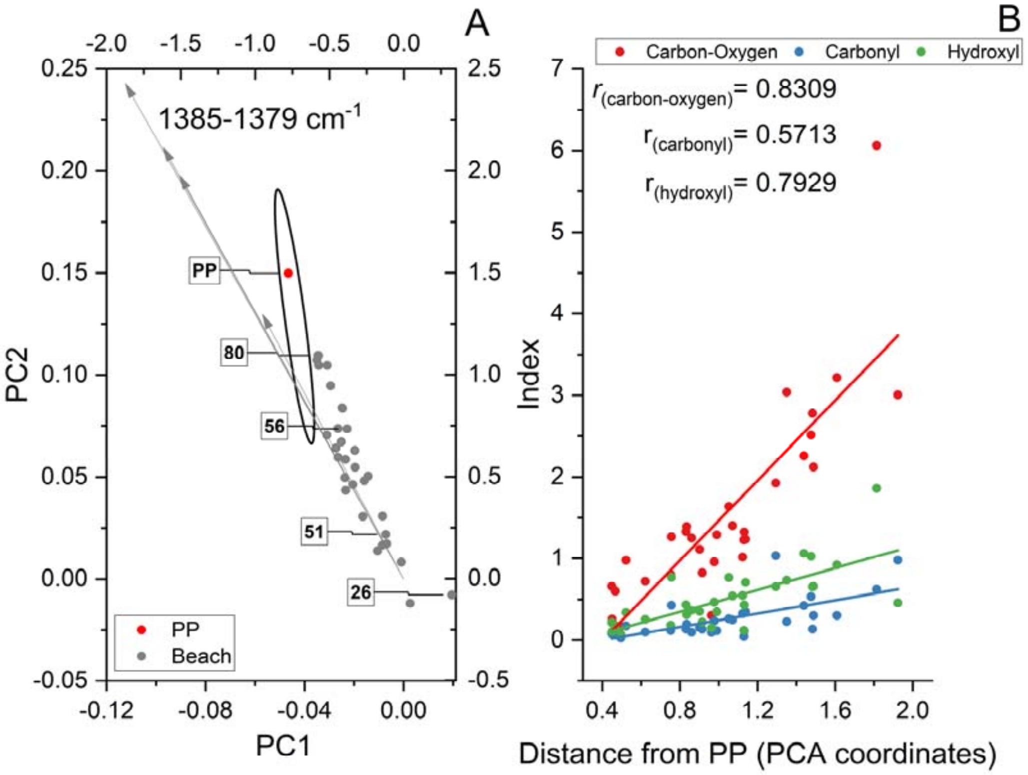

Figure 4. **A:** Location of selected beach samples in the PCA biplot with respect to the PP standard. Only samples collected in the Lucien-Blanchard Park were used as they represented most of the samples outside the PP 95% confidence ellipse. Beach samples identified by numbers were selected for further characterization. **B:** Weathering in beach samples demonstrated by the calculation of bond indexes. The distance from PP was calculated according to the PCA score coordinates in Figure 4A.

Figure 4B also shows that carbon-oxygen index was consistently higher than the two other indexes. Although the hydroxyl index is generally reported to be smaller than the carbonyl index [52], a favorable mechanism of hydrogen abstraction by alkoxyl radicals forming alcohols could support the tendency observed here. On the contrary, the high value of the carbonyl index (0.978) in the case of sample Beach-26 (distance from the PP standard in Figure 4A=1.923) may be attributed to the formation of esters as indicated by a peak observed at 1733 cm^{-1}, resulting from the decomposition of ketones and hydroperoxides, thereby decreasing the hydroxyl index at the same time. Photolytic decomposition of ketones, also known as Norrish I and Norrish II reactions, results in an increase of the carbonyl index value by forming carbon monoxide and a methyl ketone, respectively [53].

While the results obtained consisted only in a “screenshot” of the current state of materials, as erosion of small plastic pieces may later change the surface chemistry [47, 54], the results suggest that

PCA is useful to identify possible chemical weathering in plastic samples found in the environment.

3.4. Further evidence of the chemical weathering of selected beach samples

In the samples outside the PP 95% confidence ellipse of Figure 4A, even if the carbonyl peak is not as prominent as expected, characterizing some of these samples in detail can provide substantial information about the structural changes that could have occurred during the outdoor exposition of beach samples. For that reason, it was decided to select a few samples representative of that group. These samples are shown in Figure 4A (Beach-26, Beach-51, Beach-56, and Beach-80). As it can be shown, these samples are increasingly away from the PP standard in the PC1 vs PC2 biplot and it was hypothesized they would have gradual changes in their composition that explain such trend.

3.4.1. Analysis of the carbonyl region in the FTIR spectra

Many studies make use of the carbonyl index as a probe to monitor the extent of plastic weathering [55-57]. For example, Turner and Holmes [58] measured keto-carbonyl index for pellets retrieved on beaches was in accordance with their degree of yellowing, where brown-colored pellets had a roughly ten times higher index than that of the white pellets Unfortunately, it was impossible to make such a quantitative assessment regarding the degree of yellowing for each plastic particle in the present paper, as their origin was unknown.

The C=O region in FTIR was studied in detail for a representative set of samples unidentified by PCA (Beach-26, Beach-51, Beach-56, and Beach-80) and whose C=O indices are displayed in a gradient order. The aim was to confirm the weathering suggested by the bond indexes. Carbonyl stretching vibrations (1680 – 1800 cm^{-1}) are indicative of an oxidized polymer surface and gather different oxygen-containing functional groups: amide, ester, carboxylic acid, ketone, aldehyde and others. The FTIR spectra of weathered PP samples in Figure S9 (Supplementary information) confirms that these plastic debris underwent various physicochemical transformations [59].

Globally, analysis of the carbonyl region in the unprocessed FTIR spectra of the selected samples confirmed the same conclusion reached with the bond indexes. Indeed, polar functional groups formed during environmental exposure of polymer materials induced significant chemical changes relative to their initial polymeric nature, which could in part explain why they were classified as outliers in the PC1 vs PC2 biplot. However, oxygenated functions are not the only oxidation photoproducts, as scission products also result in the formation of olefins that can be observed with other spectroscopic techniques such as Raman.

3.4.2. Raman micro-spectroscopy (μ-Raman)

As μ-Raman is more adapted for the study of homoatomic bonds than FTIR, the same unidentified beach samples analyzed in the previous section were submitted to μ-Raman analysis. As shown in Figure S10 and Table S5 (Supplementary information), spectral features commonly detected for isotactic PP were also reported for the PP standard, meaning that the homopolymer was in a pure chemical state [60, 61]. Unlike the previous FTIR results, no significant changes were noticed between

PP and Beach-80 Raman spectra, as no vinyl-groups appeared to be formed in the latter. An induction period is usually observed before the vinyl content starts to increase, by the way of Norrish type II reactions [62]. This may be due in part to the presence of antioxidant additives at the polymer surface, which delay the formation of carbonyl functions, prior to their final consumption [63]. Otherwise, samples Beach-56 and Beach-51 revealed far more complex signals with an obvious rise in the proportion of olefinic unsaturations. This suggests that a great number of chain scissions occurred due to environmental exposition. Alternatively, residual monomers (i.e., propylene) trapped in PP could also explain the presence of carbon double bonds. However, this situation is unlikely to happen as unreacted propylene monomers are generally recycled throughout the polymerization process [64, 65]. Besides, the detection of chloride and/or bromide atoms in the lower frequency regions can be ascribed to the migration of halogenated additives (e.g., polybrominated diphenyl ethers, hexabromocyclododecane) towards the polymer surface, where they potentially yield brominated by-products after leaching out [66]. Compared to Beach-56 and Beach-51, no vinyl groups (≈ 1531 cm^{-1}) were detected for Beach-26, but a strong peak at ≈ 1086 cm^{-1} was evident. It indicates the presence of C–O–C bonds inside the polymer structure, in accordance with the peak at 1733 cm^{-1} in the FTIR spectra recorded for the same material (Figure S9). In fact, this wavenumber is typical of the existence of ester groups, which may have been formed after the reaction of ketones with alkoxy-radicals.

μ-Raman allowed to monitor specific vibrational bands (i.e., olefinic bands) which would not have been detected with the same intensity with FTIR. Also, this technique permits a deeper interpretation of previous results. In fact, it is possible to confirm that Norrish II reactions occurred for Beach-56 and Beach-51, but environmental exposure yielded other photoproducts (i.e., esters) in the case of Beach-26.

3.4.3. X-ray photoelectron spectroscopy (XPS)

XPS gives complementary information compared to ATR-FTIR since the former has a lower depth of analysis (≈10 nm) compared to the former (0.5 – 5 μm). For that reason, XPS was used to characterize the top surface of the four selected unidentified beach samples as well as a PP standard. Figure S11 (Supplementary information) shows the spectral survey of the selected samples. According to the quantification results in Table 2, carbon could be considered as the main constituent (C_{1s} at 285 eV) and oxygen the principal contaminant (O_{1s} at 532 eV), up to a concentration of roughly 17%. Although few other elements were detected like nitrogen (N_{1s} at 400 eV), calcium (Ca_{2p} at 347 eV), sulphur (S_{2s} at 228 eV), silicon (Si_{2s} at 153 eV) or sodium (Na_{1s} at 1072 eV), their concentrations did not exceed 3%. Contrary to FTIR data where Beach-26 was determined as the most oxidized sample, Beach-56 here had the highest oxygen amount and number of contaminants. The depth of penetration differences between ATR-FTIR and XPS techniques could explain those results. In a study based on the degradation of stacked polypropylene samples, the carbonyl absorbance only decreased after 100 μm depth, meaning that XPS analysis would have been insufficient to monitor the full degree of oxidation [67]. Another paper also reported a maximum photo-oxidation depth of 250 μm after the artificial weathering of PP [68]. Thus, XPS is only able to collect a minor fraction of the chemical information available in a weathered polymer. Nevertheless, XPS gives invaluable information on the composition of the top surface (≈8 – 10 nm) of samples, which is seen as a good indicator of the direct solar exposition of the material and it has often been probed to understand how the UV-radiation affects the formation of functional groups in PP samples [69, 70].

Table 2. Quantification results from the XPS survey spectra of standard PP and the studied unknown samples.

Sample	Atomic concentration (%)								
	C 1s	**O 1s**	**N 1s**	**Ca 2p**	**S**	**Si**	**Na**	**Fe**	**Al**
PP	≈ 100%	Trace	-	-	-	-	-	-	-
Beach-80	86.65	9.83	<1	-	-	1.53	-	<1	<1
Beach-56	75.8	17.1	1.94	<1	1.41	1.1	1.36	-	<1
Beach-51	83.37	12.21	1.5	<1	-	1.33	-	<1	<1
Beach-26	78.49	15.61	2.98	<1	-	1.43	-	<1	<1

Table 3 reports atomic concentrations (as %) associated to all homo- and heteroatomic carbon bonds determined from C_{1s} high-resolution spectra (Figure S12A, Supplementary information). The proportion of carbon-oxygen bonds (i.e., the oxidized part) increases steadily by contrast to those of the saturated hydrocarbons.

Table 3. Quantification results from the C_{1s} high-resolution spectra of standard PP and the selected beach samples.

Sample	Bond concentration (%)					
	C-C	**C=C**	**C-O-C/C-OH**	**C=O**	**COOH**	**O=C-N-C=O**
PP	98.56	0.39	1.05	-	-	-
Beach-80	93.50	0.34	3.55	0.89	0.92	0.79
Beach-56	86.93	1.36	6.14	1.35	1.42	2.80
Beach-51	83.79	4.77	6.51	1.50	1.07	2.36
Beach-26	83.57	2.33	7.66	1.96	1.20	3.28

A mechanism has already been proposed to explain the formation of alcohol-groups for ultra-high molecular weight polyethylene [71]. Briefly, peroxy-radicals formed at the subsurface react with each other to give a carbonyl-group and an alcohol-group. Except for Beach-26, the linearity between vinyl-groups and carbonyl-groups was evident, proving that chain scissions mainly occurred within polymers by Norrish II reactions [72]. In the case of Beach-26, it is possible that the abundance of vinylidene groups decreased after a subsequent oxidation into carbonyl-groups. This assumption is supported by Yanai, *et al.* [73] who found a higher vinylidene content in the inner layers than at the outer layers after 286 h of UV-irradiation, by contrast to that of the carbonyl groups which was highest at the surface. Finally, the quantity of carbon-nitrogen bonds was consistent to the spectral survey results.

Table 4 shows the bond concentrations (%) associated to oxygen bonds determined from O_{1s} high-resolution spectra (Figure S12B, Supplementary information). Two important trends can be observed in this table. First, the increase of C-$\underline{O}$ bonds along weathering is similar to previous results (Table 3). Moreover, the ratio of C-$\underline{O}$ *versus* C=$\underline{O}$ bonds follows the same trend and might account for esters formation through photolysis of in-chain ketones by alkoxy radicals [74]. Second, a decrease in the charging effects is explained by the concomitant increase of surface polar functional groups (e.g., alcohols, esters, ketones), which affect the electronic properties of the polymer via the introduction of new electrical dipoles [69].

Table 4. Quantification results from the O_{1s} high-resolution spectra of standard PP and the selected beach samples.

Sample	Bond concentration (%)			
	Charge effect	C=O	C-O-C/C-OH	O-C=O
PP	-	-	-	-
Beach-80	7.78	46.54	39.93	5.75
Beach-56	7.25	36.51	45.87	9.11
Beach-51	4.95	32.52	40.90	21.63
Beach-26	2.68	22.85	47.75	26.73

Overall, XPS turned out to be a very efficient technique for the quantification of specific chemical bonds at the top layer, which cannot be selectively probed by Raman or FTIR. XPS spectral survey results sometimes contrasted with those of FTIR, where Beach-56 was deemed as the most oxidized unidentified sample, instead of Beach-26. Otherwise, the conclusions drawn with FTIR and µ-Raman spectroscopy, indicating that except for Beach-26, Norrish II reactions seemed to have taken place mostly at the surface of unidentified plastics, were quite similar with XPS. In addition, according to O_{1s} high-resolution spectra, ester group concentration was the highest for Beach-26, supporting FTIR observations.

3.4.4. Scanning Electron Microscopy (SEM)

All the structural modifications discussed earlier generate numerous cracks, pits and/or flakes at the surface of the polymers, rendering the material more brittle [75, 76]. The current state of the material's surface may therefore reflect the extent of polymer degradation. Then, irregularities in the first polymeric layer should become more and more pronounced as we move away from the PP cluster. Of all the analytical techniques employed to picture the surface topology of plastics, SEM is one of the most represented [77]. Thus, SEM was used to confirm that the surface of the selected unidentified beach samples agreed with their degree of chemical weathering.

The level of physical and chemical weathering of the selected beach samples (Figure S13, Supplementary information) was consistent with previous results. The less weathered Beach-80 and Beach-56 beach samples showed grooves along their upper surfaces (Figure S13B) suggesting previous sedimentological processes such as saltation, where plastic particles may have come into contact with sand grains [78]. As these processes are only of mechanical nature, it is therefore not expected that these samples contain a high oxygen content. However, the XPS survey spectra results shown in Table 2 indicated that Beach-56 was the most oxidized of the unidentified beach samples, with almost 25% (O/C=0.23) of oxygen amount. A closer look at the particle section (magnification 200×) revealed the existence of numerous solution pits, which are well known to contain oxidation textures within or around them [79]. Therefore, it was hypothesized that Beach-56 was mostly oxidized on the edges than in the upper surface, a tendency also observed by Corcoran, *et al.* [80]. In fact, they reported that particle margins were favorable sites of oxidation, as for linear fractures, with a positive correlation existing between the extent of mechanical weathering textures and the degree of chemical oxidation. Besides, samples Beach-51 (Figure S13C) and Beach-26 (Figure S13D) displayed more complex degradation patterns in their upper surfaces such as flakes and even a vermiculate texture (magnification 30×), whose presence for the latter is indicative of extended chemical weathering. Consequently, Beach-26 may have experienced prolonged exposure time in the beach environment than in the solution environment, as the level of UV-radiation and mechanical erosion is minimal in rivers, compared to beaches. Finally, SEM images confirmed that Beach-26 was the most oxidized of the selected beach samples, followed closely by Beach-56 and Beach-51 samples, whereas Beach-80 upper surface seemed to have only undergone mechanical weathering (results not shown).

4. Conclusions

PCA and HCA of preprocessed infrared spectra of plastic debris found on public beaches showed that samples can be associated with known polymers, but a clear identification was not always possible. About 60% of the beach samples were classified as outliers by PCA. However all of them were classified by HCA as one of the five targeted polymers in this study (PE, PP, PS, PET, and PVC).

Analysis by an array of complementary techniques (FTIR, μ-Raman, XPS, SEM) of beach samples classified as outliers to PP in PCA showed that weathering was found to be the main cause of uncertain identification of beach samples, however, in some cases the presence of copolymers and additives cannot be completely ruled out. While results showed that μ-Raman, XPS and SEM were necessary to comprehend more readily the nature the phenomena responsible for the transformation of samples, this study shows that PCA and HCA of preprocessed IR spectra could be used for fast screening of polymer weathering in environmental samples.

Future experiments should focus on the applicability of the proposed combined chemometric approach for very small microplastics (<100 μm), as they have more important effects than larger plastics on aquatic ecosystems.

5. Acknowledgements

This study was supported by the Natural Sciences and Engineering Research Council of Canada (NSERC) and the Fonds de recherche du Québec – Nature et technologies (FRQNT). The authors would like to acknowledge the financial support the Environmental Decontamination Technologies and Integrated Water and Wastewater Management (TEDGIEER) NSERC CREATE program for N. Nayrac's scholarship. The authors thank Paul-Ludovic Karsenti, René Gagnon, Adrien Schlachter, Sonia Blais and Denis Morris for their technical assistance with the characterisation techniques and Marie-Audrey Lett for her contribution to sampling.

CRediT author statement

Nicolas Nayrac: Conceptualization, Formal analysis, Investigation, Methodology, Software, Validation, Visualization, Writing – Original Draft, Writing – Review & Editing
Jean-Philippe Bellenger Supervision, Writing – Review & Editing
Pedro A. Segura: Conceptualization, Funding Acquisition, Methodology, Resources, Supervision, Writing – Review & Editing, Project administration

6. *References*

1. W. J. Shim and R. C. Thomposon, *Arch. Environ. Contam. Toxicol.*, 2015, **69**, 265-268.
2. L. Su, Y. Xue, L. Li, D. Yang, P. Kolandhasamy, D. Li and H. Shi, *Environ. Poll.*, 2016, **216**, 711-719.
3. A. Crew, I. Gregory-Eaves and A. Ricciardi, *Environ. Poll.*, 2020, **260**, 113994.
4. Y. Zhou, J. Wang, M. Zou, Z. Jia, S. Zhou and Y. Li, *Sci. Total Environ.*, 2020, **748**, 141368.
5. J. Frias, P. Sobral and A. M. Ferreira, *Mar. Pollut. Bull.*, 2010, **60**, 1988-1992.
6. R. Dris, J. Gasperi, M. Saad, C. Mirande and B. Tassin, *Mar. Pollut. Bull.*, 2016, **104**, 290-293.
7. I. Peeken, S. Primpke, B. Beyer, J. Gütermann, C. Katlein, T. Krumpen, M. Bergmann, L. Hehemann and G. Gerdts, *Nat. Commun.*, 2018, **9**, 1-12.
8. Y. Mato, T. Isobe, H. Takada, H. Kanehiro, C. Ohtake and T. Kaminuma, *Environ. Sci. Technol.*, 2001, **35**, 318-324.
9. M. Oliveira, A. Ribeiro, K. Hylland and L. Guilhermino, *Ecol. Indic.*, 2013, **34**, 641-647.
10. A. Karami, N. Romano, T. Galloway and H. Hamzah, *Environmental research*, 2016, **151**, 58-70.
11. O. Guven, L. Bach, P. Munk, K. V. Dinh, P. Mariani and T. G. Nielsen, *Aquat. Toxicol.*, 2018, **198**, 287-293.
12. W. Huang, B. Song, J. Liang, Q. Niu, G. Zeng, M. Shen, J. Deng, Y. Luo, X. Wen and Y. Zhang, *J. Hazard. Mater.*, 2021, **405**, 124187.
13. K. Bucci, M. Tulio and C. Rochman, *Ecological Applications*, 2020, **30**, e02044.
14. A. L. Andrady, *Mar. Pollut. Bull.*, 2017, **119**, 12-22.
15. A. Müller, R. Becker, U. Dorgerloh, F.-G. Simon and U. Braun, *Environ. Poll.*, 2018, **240**, 639-646.
16. F. Mammo, I. Amoah, K. Gani, L. Pillay, S. Ratha, F. Bux and S. Kumari, *Sci. Total Environ.*, 2020, **743**, 140518.
17. G. Liu, Z. Zhu, Y. Yang, Y. Sun, F. Yu and J. Ma, *Environ. Poll.*, 2019, **246**, 26-33.
18. X. Wu, P. Liu, H. Huang and S. Gao, *Sci. Total Environ.*, 2020, **717**, 137033.
19. M. R. Jung, F. D. Horgen, S. V. Orski, V. Rodriguez, K. L. Beers, G. H. Balazs, T. T. Jones, T. M. Work, K. C. Brignac and S.-J. Royer, *Mar. Pollut. Bull.*, 2018, **127**, 704-716.
20. S. Huppertsberg and T. P. Knepper, *Anal. Bioanal. Chem.*, 2018, **410**, 6343-6352.
21. B. Duarte, D. Prata, A. R. Matos, M. T. Cabrita, I. Caçador, J. C. Marques, H. N. Cabral, P. Reis-Santos and V. F. Fonseca, *Sci. Total Environ.*, 2019, **650**, 2085-2094.
22. W. Cowger, A. Gray, S. H. Christiansen, H. DeFrond, A. D. Deshpande, L. Hemabessiere, E. Lee, L. Mill, K. Munno and B. E. Ossmann, *App. Spectrosc.*, 2020, **74**, 989-1010.

23. C. F. Araujo, M. M. Nolasco, A. M. Ribeiro and P. J. Ribeiro-Claro, *Water Res.*, 2018, **142**, 426-440.
24. B. E. Oßmann, G. Sarau, S. W. Schmitt, H. Holtmannspötter, S. H. Christiansen and W. Dicke, *Anal. Bioanal. Chem.*, 2017, **409**, 4099-4109.
25. G. Renner, A. Nellessen, A. Schwiers, M. Wenzel, T. C. Schmidt and J. Schram, *TrAC Trends in Analytical Chemistry*, 2019, **111**, 229-238.
26. L. Cabernard, L. Roscher, C. Lorenz, G. Gerdts and S. Primpke, *Environ. Sci. Technol.*, 2018, **52**, 13279-13288.
27. H. De Frond, R. Rubinovitz and C. M. Rochman, *Anal. Chem.*, 2021, **93**, 15878-15885.
28. S. Primpke, M. Wirth, C. Lorenz and G. Gerdts, *Anal. Bioanal. Chem.*, 2018, **410**, 5131-5141.
29. V. H. da Silva, F. Murphy, J. M. Amigo, C. Stedmon and J. Strand, *Anal. Chem.*, 2020, **92**, 13724-13733.
30. M. Zvekic, L. C. Richards, C. C. Tong and E. T. Krogh, *Environ. Sci. Process Impacts*, 2022, **24**, 52-61.
31. J. M. Andrade, B. Ferreiro, P. López-Mahía and S. Muniategui-Lorenzo, *Mar. Pollut. Bull.*, 2020, **154**, 111035.
32. W. Cowger, A. M. Booth, B. M. Hamilton, C. Thaysen, S. Primpke, K. Munno, A. L. Lusher, A. Dehaut, V. P. Vaz and M. Liboiron, *App. Spectrosc.*, 2020, **74**, 1066-1077.
33. C. Kirchkeszner, N. Petrovics, T. Tábi, N. Magyar, J. Kovács, B. S. Szabó, Z. Nyiri and Z. Eke, *Food Control*, 2022, **132**, 108354.
34. R. Gautam, S. Vanga, F. Ariese and S. Umapathy, *EPJ Tech. Instrum.*, 2015, **2**, 1-38.
35. M. De Luca, W. Terouzi, G. Ioele, F. Kzaiber, A. Oussama, F. Oliverio, R. Tauler and G. Ragno, *Food Chem.*, 2011, **124**, 1113-1118.
36. M. Rodrigues, N. Abrantes, F. Gonçalves, H. Nogueira, J. Marques and A. Gonçalves, *Sci. Total Environ.*, 2018, **633**, 1549-1559.
37. J. Wang, J. Peng, Z. Tan, Y. Gao, Z. Zhan, Q. Chen and L. Cai, *Chemosphere*, 2017, **171**, 248-258.
38. L. Yang, Y. Zhang, S. Kang, Z. Wang and C. Wu, *Sci. Total Environ.*, 2021, **754**, 141948.
39. L. A. Rasmussen, L. Iordachescu, S. Tumlin and J. Vollertsen, *Water Res.*, 2021, **201**, 117307.
40. R. Bro and A. K. Smilde, *Anal. Methods*, 2014, **6**, 2812-2831.
41. T. Ojeda, A. Freitas, K. Birck, E. Dalmolin, R. Jacques, F. Bento and F. Camargo, *Polym. Degrad. Stab*, 2011, **96**, 703-707.
42. Plastics Europe, Plastics - The Facts 2021, https://plasticseurope.org/knowledge-hub/plastics-the-facts-2021/, (accessed 2022-06-02, 2022).
43. Y. Sun, J. Yuan, T. Zhou, Y. Zhao, F. Yu and J. Ma, *Environ. Poll.*, 2020, **265**, 114864.
44. M. Zvekic, L. C. Richards, C. C. Tong and E. T. Krogh, *Environ. Sci. Process Impacts*, 2022.
45. G. Grause, M.-F. Chien and C. Inoue, *Polym. Degrad. Stab*, 2020, **181**, 109364.
46. R. N. Jones and A. Cole, *J. Am. Chem. Soc.*, 1952, **74**, 5648-5661.
47. J. Brandon, M. Goldstein and M. D. Ohman, *Mar. Pollut. Bull.*, 2016, **110**, 299-308.
48. A. Martínez-Romo, R. González-Mota, J. Soto-Bernal and I. Rosales-Candelas, *J. Spectrosc.*, 2015, **2015**.

49. Y. Ángeles-López, A. Gutiérrez-Mayen, M. Velasco-Pérez, M. Beltrán-Villavicencio, A. Vázquez-Morillas and M. Cano-Blanco, *J. Phys.: Conf. Ser.*, 2017, **792**, 012027.
50. V. Mylläri, T. P. Ruoko and S. Syrjälä, *J. Appl. Polym. Sci.*, 2015, **132**.
51. J. Almond, P. Sugumaar, M. N. Wenzel, G. Hill and C. Wallis, *e-Polymers*, 2020, **20**, 369-381.
52. C. Rouillon, P.-O. Bussiere, E. Desnoux, S. Collin, C. Vial, S. Therias and J.-L. Gardette, *Polym. Degrad. Stab*, 2016, **128**, 200-208.
53. A. Chamas, H. Moon, J. Zheng, Y. Qiu, T. Tabassum, J. H. Jang, M. Abu-Omar, S. L. Scott and S. Suh, *ACS Sustainable Chemistry & Engineering*, 2020, **8**, 3494-3511.
54. A.-M. Resmeriță, A. Coroaba, R. Darie, F. Doroftei, I. Spiridon, B. C. Simionescu and P. Navard, *Mar. Pollut. Bull.*, 2018, **127**, 387-395.
55. A. Ter Halle, L. Ladirat, X. Gendre, D. Goudouneche, C. Pusineri, C. Routaboul, C. Tenailleau, B. Duployer and E. Perez, *Environ. Sci. Technol.*, 2016, **50**, 5668-5675.
56. J. C. Prata, V. Reis, A. Paço, P. Martins, A. Cruz, J. P. da Costa, A. C. Duarte and T. Rocha-Santos, *Sci. Total Environ.*, 2020, **709**, 135892.
57. A. Beltrán-Sanahuja, N. Casado-Coy, L. Simó-Cabrera and C. Sanz-Lázaro, *Environ. Poll.*, 2020, **259**, 113836.
58. A. Turner and L. Holmes, *Mar. Pollut. Bull.*, 2011, **62**, 377-381.
59. M. Dong, Q. Zhang, X. Xing, W. Chen, Z. She and Z. Luo, *Sci. Total Environ.*, 2020, **739**, 139990.
60. E. Andreassen, in *Polypropylene*, Springer, 1999, pp. 320-328.
61. M. A. De Baez, P. Hendra and M. Judkins, *Spectrochim. Acta A Mol. Biomol. Spectrosc.*, 1995, **51**, 2117-2124.
62. N. M. Stark and L. M. Matuana, *Polym. Degrad. Stab*, 2004, **86**, 1-9.
63. V. Ambrogi, P. Cerruti, C. Carfagna, M. Malinconico, V. Marturano, M. Perrotti and P. Persico, *Polym. Degrad. Stab*, 2011, **96**, 2152-2158.
64. B. Jiang, H. Shao, H. Nie and A. He, *Polym. Chem.*, 2015, **6**, 3315-3323.
65. H. A. Maddah, *Am. J. Polym. Sci*, 2016, **6**, 1-11.
66. M. Ateia, A. Kanan and T. Karanfil, *Chemosphere*, 2020, **251**, 126452.
67. P. Gijsman, G. Meijers and G. Vitarelli, *Polym. Degrad. Stab*, 1999, **65**, 433-441.
68. T. Grossetete, L. Gonon and V. Verney, *Polym. Degrad. Stab*, 2002, **78**, 203-210.
69. A. Rjeb, S. Letarte, L. Tajounte, M. C. El Idrissi, A. Adnot, D. Roy, Y. Claire and J. Kaloustian, *J. Electron Spectros. Relat. Phenomena*, 2000, **107**, 221-230.
70. S. Massey, D. Roy and A. Adnot, *Nucl. Instrum. Methods Phys. Res. B: Beam Interact. Mater. At.*, 2003, **208**, 236-241.
71. S. Lu, F. Buchanan and J. Orr, *Polymer Testing*, 2002, **21**, 623-631.
72. S. A. Jabarin and E. A. Lofgren, *J. Appl. Polym. Sci.*, 1994, **53**, 411-423.
73. G. Yanai, A. Ram and J. Miltz, *J. Appl. Polym. Sci.*, 1996, **59**, 1145-1149.
74. G. Geuskens and M. Kabamba, *Polym. Degrad. Stab*, 1982, **4**, 69-76.
75. J. Gulmine, P. Janissek, H. Heise and L. Akcelrud, *Polym. Degrad. Stab*, 2003, **79**, 385-397.
76. L. Cai, J. Wang, J. Peng, Z. Wu and X. Tan, *Sci. Total Environ.*, 2018, **628**, 740-747.
77. S. Mariano, S. Tacconi, M. Fidaleo, M. Rossi and L. Dini, *Frontiers in Toxicology*, 2021, **3**, 636640.
78. D. A. Cooper and P. L. Corcoran, *Mar. Pollut. Bull.*, 2010, **60**, 650-654.

79. M. Zbyszewski and P. L. Corcoran, *Water Air Soil Poll.*, 2011, **220**, 365-372.
80. P. L. Corcoran, M. C. Biesinger and M. Grifi, *Mar. Pollut. Bull.*, 2009, **58**, 80-84.